Journal of Alloys and Compounds 551 (2013) 61–66

Contents lists available at SciVerse ScienceDirect

Journal of Alloys and Compounds

journal homepage: www.elsevier.com/locate/jalcom

Enhanced superplasticity in friction stir processed Mg–Gd–Y–Zr alloy

Q. Yang, B.L. Xiao *, Z.Y. Ma *

Shenyang National Laboratory for Materials Science, Institute of Metal Research, Chinese Academy of Sciences, 72 Wenhua Road, Shenyang 110016, China

ARTICLE INFO

Article history:
Received 23 June 2012
Received in revised form 27 September 2012
Accepted 2 October 2012
Available online 11 October 2012

Keywords:
Friction stir processing
Magnesium alloy
Precipitation
Superplasticity

ABSTRACT

Fine-grained supersaturated Mg–10Gd–3Y–0.5Zr (GW103) alloy with predominant high-angle grain boundaries (HAGB) was prepared by friction stir processing (FSP). The FSP GW103 alloy was subjected to superplastic investigation at a small temperature range of 400–425 °C. Fine β-Mg_5(Gd,Y) particles precipitated at the grain boundaries during heating before superplastic deformation, and their volume fraction decreased significantly with increasing the temperature from 400 to 425 °C. Superplasticity of the FSP GW103 alloy was sensitive to the testing temperature, and a maximum superplasticity of 1110% was achieved at 1×10^{-3} s^{-1} and a medium temperature of 415 °C. Grain boundary sliding was identified as the main deformation mechanism in FSP GW103 alloy. The high superplasticity is attributed to the fine grains, high percentage of HAGBs, and a moderate volume fraction of β particles that precipitated at 415 °C.

1. Introduction

The addition of rare-earth elements (RE) into the magnesium alloys has been widely investigated with the aim to develop high-strength magnesium alloys [1–3]. Among them, the equilibrium solid solubility of Gd in Mg is relatively high, and the Mg–Gd alloys are considered promising candidates for high-strength magnesium alloys via precipitation hardening [4,5]. In recent years, considerable efforts have been made to explore high strength in the Mg–Gd based alloys by either adjusting the alloying elements or optimizing the processing methods including plastic deformation and heat treatment [1,2,5–9].

Li et al. [2] developed a high strength Mg–14Gd–0.5Zr (wt.%) alloy with a tensile strength of 482 MPa via combined processes of extrusion, rolling and aging. Furthermore, a high tensile strength of 542 MPa was achieved in a hot extruded Mg–1.8Gd–1.8Y–0.7Zn–0.2Zr (mol.%) alloy [1]. However, the ductility of these alloys was poor, and their formability was then a problem in industrial applications. Superplastic forming is an effective method of fabricating these hard-to-form materials into complex shapes [10].

Until now, quite limited studies were available on the superplasticity of the Mg–Gd based alloys [11–14]. Zhang et al. [11,13] observed the superplastic behavior of Mg–Gd–Y–Zr alloy, and the maximum elongation was 410% at 450 °C and 2×10^{-4} s^{-1} and 380% at 435 °C and 5×10^{-4} s^{-1} for the extruded bar and rolling sheet, respectively. Their studies revealed that, superplasticity could be achieved in both fine- and coarse-grained Mg–9Gd–4Y–0.4Zr (wt.%) alloys, as the cuboidal-shaped Mg_3Gd particles and the irregular-shaped β-Mg_5(Gd,Y) particles that precipitated during superplastic deformation exhibited significant pinning effect on the grain boundaries. Kulyasova et al. [14] prepared an ultrafine-grained (UFG) Mg–10Gd (wt.%) alloy with a grain size <100 nm by high pressure torsion (HPT), and a maximum elongation of 580% was obtained at 400 °C and 1×10^{-3} s^{-1}. However, both the maximum superplastic elongation and the optimum superplastic strain rate of the Mg–Gd based alloys were lower compared with other superplastic magnesium alloys [15–17]. Reasons for these may be due to the existence of the second-phase particles.

It is well documented that the thermally stable second-phase particles are crucial for enhancing superplasticity, as they can stabilize the grains during superplastic deformation [18,19]. However, on the other hand, a large volume fraction of particles, in particular large-sized particles could cause cavitation as large local stress concentration was generated around the particles. In this case, the particles were not beneficial to superplasticity. Therefore, it is necessary to control the number and size of second-phase particles both prior to and during superplastic deformation to obtain enhanced superplasticity.

Li et al. [20] observed the precipitation of the grain boundary particles after compression at 400 °C in an extruded Mg–8Gd–3Y–0.5Zr (wt.%) alloy, while these particles were not detected when compressed at 425 °C. This implies that the precipitation of second-phase particles in the Mg–Gd–Y–Zr alloys is very sensitive to the deformation temperature, therefore the particle pinning effect may vary with the temperature. It is expected that high

* Corresponding authors. Tel.: +86 24 83978630; fax: +86 24 23971749 (B.L. Xiao); tel./fax: +86 24 83978908 (Z.Y. Ma).
E-mail addresses: blxiao@imr.ac.cn (B.L. Xiao), zyma@imr.ac.cn (Z.Y. Ma).

0925-8388/$ - see front matter © 2012 Elsevier B.V. All rights reserved.
http://dx.doi.org/10.1016/j.jallcom.2012.10.002

superplasticity could be achieved by controlling the particle precipitation through adjusting the deformation temperature. However, the study on the effect of particle precipitation on superplasticity of the Mg–Gd based alloys is lacking.

Our previous studies indicated that fine-grained Mg–10Gd–3Y–0.5Zr (GW103) alloy could be produced by friction stir processing (FSP) technique [21,22]. The FSP GW103 alloy exhibited significantly enhanced mechanical properties compared to its cast counterpart. In this study, the superplastic behavior of the FSP fine-grained GW103 alloy was investigated at a small temperature range of 400–425 °C. The aim is (a) to understand the effect of particle precipitation during deformation on the superplasticity and (b) to achieve high superplasticity.

2. Experimental

Eight millimeter thick Mg–10Gd–3Y–0.5Zr (wt.%) cast plate was subjected to FSP at a rotation rate of 800 rpm and a traverse speed of 50 mm min^{-1}. A tool with a shoulder 20 mm in diameter, a threaded conical pin 8 mm in root diameter and 6 mm in length was used. Microstructural characterization was performed by optical microscopy (OM) and transmission electron microscopy (TEM). The volume fractions of second-phase particles were analyzed by an image analysis software (Image-Pro Plus 6.0). Electron backscatter diffraction (EBSD) orientation map was obtained using a ZEISS SUPRA 35. Specimen for the EBSD observation was electro-polished in commercial AC2 electrolyte at 25 V and 20 °C.

Mini tensile specimens (2.5 mm gage length, 1.4 mm gage width and 1.0 mm gage thickness) were machined in the cross section perpendicular to the FSP direction with the gage length being centered in the process zone. The specimens were subsequently ground and polished to a final thickness of 0.8 mm. Tensile tests were carried out using an Instron 5848 microtester. The specimens were heated to the testing temperature and then held at that temperature for 20 min to establish thermal equilibrium before tensile test.

3. Results

Fig. 1 shows the microstructure of the cast and FSP GW103 alloys. The cast alloy was characterized by the coarse grains and the grain boundary eutectic $Mg_5(Gd,Y)$ networks (Fig. 1(a)). By comparison, the fine and equiaxed grains with an average grain size of 6.1 μm and a supersaturated magnesium matrix were obtained after FSP (Fig. 1(b)) as reported previously [21]. Fig. 2(a) shows the orientation map of the FSP GW103 alloy, where high-angle grain boundaries (HAGBs, grain boundary misorientations $\geqslant 15°$) and low-angle grain boundaries (LAGBs, grain boundary misorientations $<15°$) are depicted by black and white lines, respectively. The microstructure was characterized by equiaxed grains with predominant HAGBs, and the fraction of the HAGBs was determined to be 93% (Fig. 2(b)).

Fig. 3(a) and (b) shows the true stress–true strain curves of the FSP GW103 alloy at an initial strain rate of 1×10^{-3} s^{-1} for temperatures of 400–425 °C and at 415 °C for different strain rates ranging from 1×10^{-4} to 3×10^{-3} s^{-1}, respectively. At a strain rate of 1×10^{-3} s^{-1}, the optimum temperature for maximum elongation was determined to be 415 °C, and at 415 °C, the optimum strain rate was 1×10^{-3} s^{-1}. A strain softening occurred at lower temperatures and higher strain rates, while at increased temperatures or decreased strain rates, this strain softening changed into a slight strain hardening.

Fig. 4(a) shows the variation of elongation with the initial strain rate at various temperatures for the FSP GW103 alloy. It is evident that the elongation was sensitive to both the temperature and strain rate. A maximum elongation of 1110% was achieved at 415 °C and 1×10^{-3} s^{-1}. Fig. 4(b) shows the variation of flow stress (at true strain of 0.1) with the initial strain rate at various temperatures for the FSP GW103 alloy. The strain rate sensitivity m of ~0.5 was observed in the investigated strain rate ranges for all temperatures.

Fig. 5 shows the tested specimens of the FSP GW103 alloy deformed to failure at 415 °C for different strain rates. All the specimens show relatively uniform elongation that is characteristic of superplastic flow.

Fig. 6(a)–(c) shows the microstructure of the FSP GW103 alloy before deformation (heated to the testing temperatures and held for 20 min, hereafter referred to annealed samples) at 400, 415 and 425 °C, respectively. Compared to that in the as-FSP sample (Fig. 1(b)), large numbers of particles with an average size of ~1 μm were precipitated at the grain boundaries in the annealed samples. The particle volume fraction decreased with increasing the annealing temperature, and was estimated to be 20.4%, 14.3% and 4.1% at 400, 415 and 425 °C, respectively. The number of particles in the sample annealed at 425 °C was much lower than that annealed at 400 °C. In addition, the average grain size of the FSP GW103 alloy was fundamentally unchanged after annealing at different temperatures.

Fig. 6(d)–(f) shows the microstructure in the gage region of the tensile specimens deformed to failure at a fixed strain rate of 1×10^{-3} s^{-1} for 400, 415 and 425 °C, respectively, which correspond to the deformation time of about 1.3, 3.1 and 2.1 h at 400, 415 and 425 °C, respectively. The grain boundary particles experienced obvious growth during superplastic deformation, and the average particle size increased up to ~3 μm at 415 and 425 °C. In addition, dynamic grain growth occurred during superplastic deformation at all temperatures. The average grain size in the longitudinal and traverse directions increased to 15.7 μm and 8.4 μm at 400 °C, 19.6 μm and 11.3 μm at 415 °C, and 25.1 μm and 16.2 μm at 425 °C, respectively.

Furthermore, large-sized cavities with an irregular shape were frequently observed in the tensile specimens deformed at 400 and 425 °C (Fig. 6(d) and (f)). However, the cavities were rarely observed and the cavity size was very small in the sample deformed at 415 °C (Fig. 6(e)).

Fig. 7 shows the TEM image of the annealed sample at 400 °C. The precipitated particles were only distributed at the grain

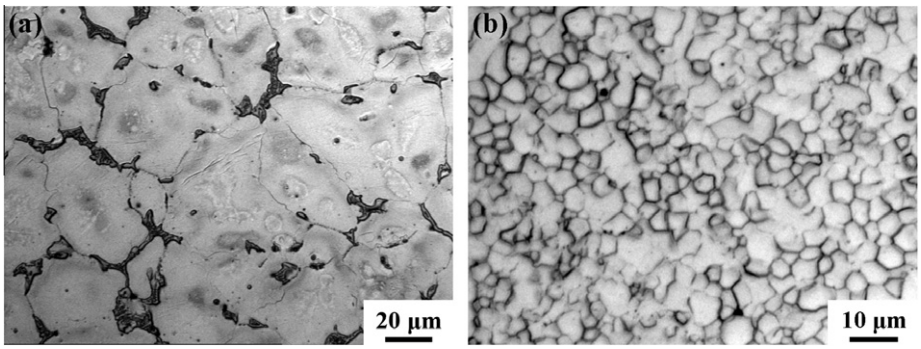

Fig. 1. Microstructure of (a) cast and (b) FSP GW103 alloys.

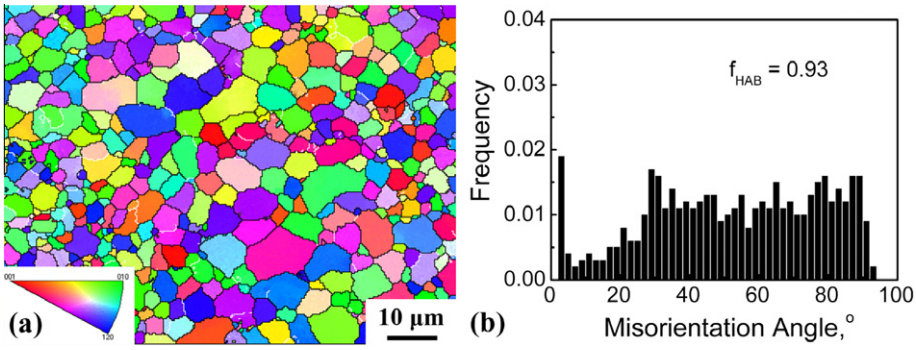

Fig. 2. Microstructure of FSP GW103 alloy: (a) EBSD map and (b) boundary misorientation angle distribution.

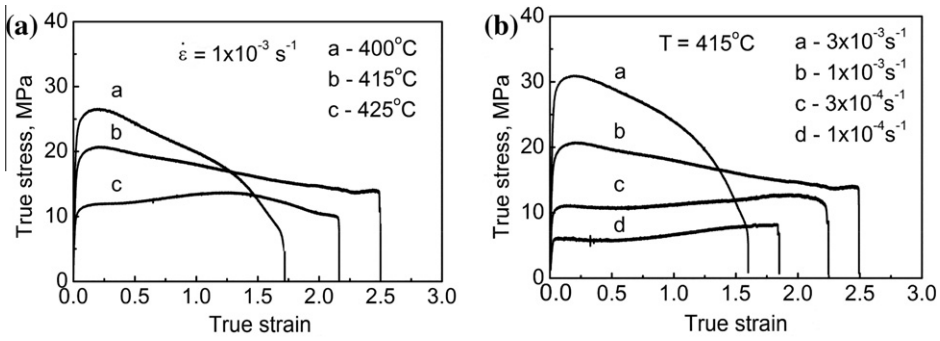

Fig. 3. Effect of (a) temperature and (b) strain rate on true stress–true strain curves of FSP GW103 alloy.

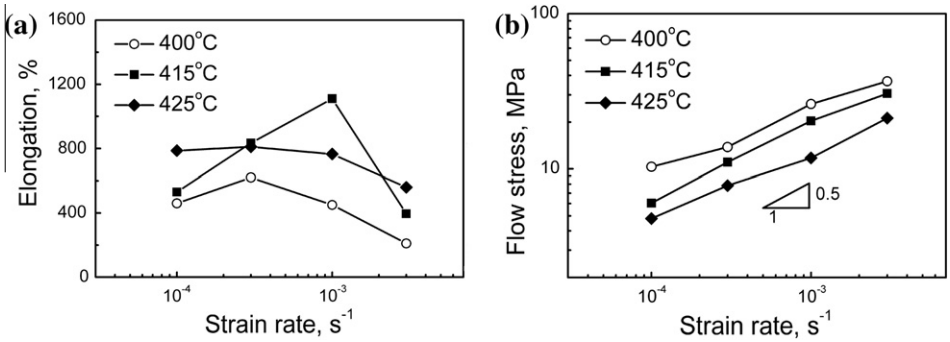

Fig. 4. Variation of (a) elongation and (b) flow stress with initial strain rate for FSP GW103 alloy.

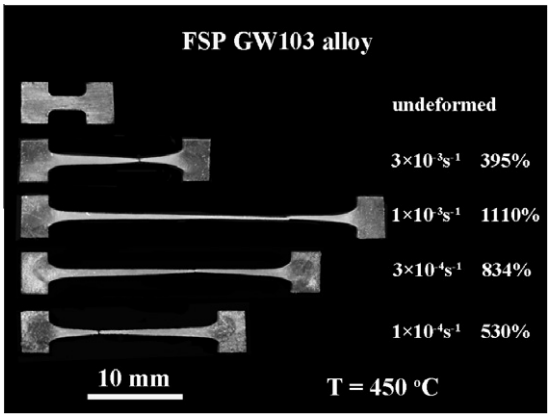

Fig. 5. Tensile specimens pulled to failure at 415 °C.

boundaries, and no precipitates were observed inside the grains. These grain boundary particles were identified as the β-Mg_5(Gd,Y), as indicated by the selected area electron diffraction (SAED) patterns.

Fig. 8 shows the surface morphology of the FSP GW103 alloy deformed to failure at 415 °C and an initial strain rate of 1×10^{-3} s^{-1}. Pronounced striated bands (SB) with a large width (as indicated by arrows) and irregular cracks were frequently observed.

4. Discussion

4.1. Microstructural characteristics

It is well documented that severe plastic deformation was generated at high temperature during FSP. This resulted in significant grain refinement through dynamic recrystallization, and considerable dissolution of second-phase particles due to remarkably accelerated diffusion rate in the magnesium alloy castings. Therefore,

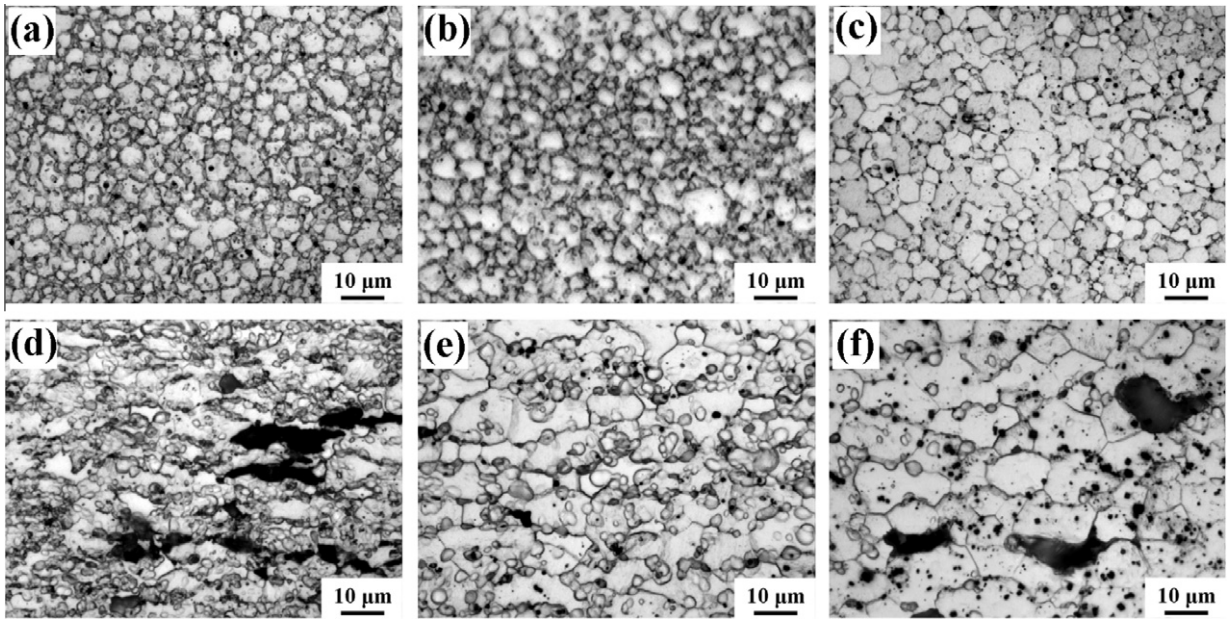

Fig. 6. Microstructure of FSP GW103 alloy before (a–c) and after (d–f) superplastic deformation at 1×10^{-3} s^{-1} and different temperatures: (a), (d) 400 °C, (b), (e) 415 °C and (c), (f) 425 °C.

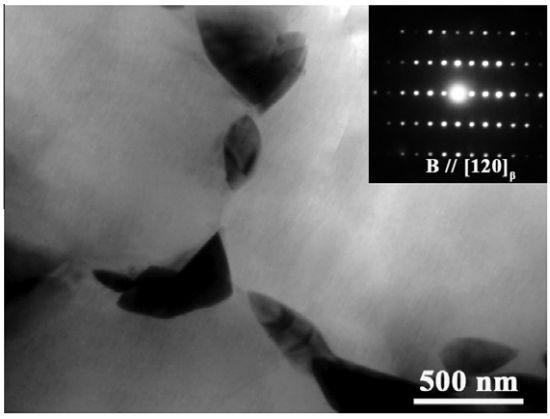

Fig. 7. TEM image of FSP GW103 alloy before superplastic deformation at 400 °C.

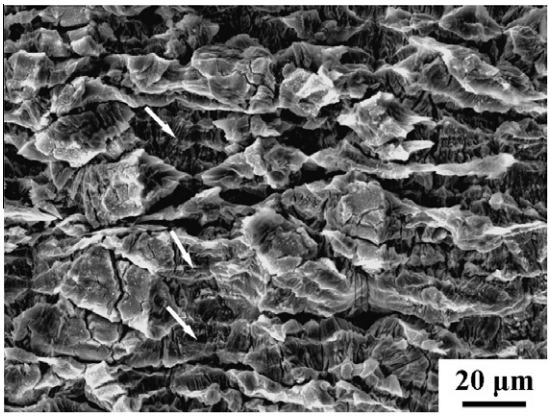

Fig. 8. Surface morphology of FSP GW103 sample deformed to failure at 415 °C and 1×10^{-3} s^{-1} (tensile axis is horizontal).

like the typical microstructure in other FSP magnesium castings [16,23], the fine-grained supersaturated structure with the predominant HAGBs was produced in the FSP GW103 alloy.

Our previous study indicated that, after heating to about 350 °C, the precipitation of the stable β-Mg_5(Gd,Y) phase occurred in the FSP GW103 alloy [21]. In the present study, the fine β particles were observed to precipitate at the grain boundaries in the annealed samples with the annealing temperatures of 400–425 °C (Fig. 6(a)–(c)). This was consistent with the previous study [21].

Note that Li et al. [20] did not observe the precipitates in an extruded Mg–8Gd–3Y–0.5Zr (wt.%) alloy after heating from room temperature to test temperatures of 400–490 °C and holding at those temperatures for 15 min. The accelerated precipitation behavior in the FSP GW103 alloy compared with that in the extruded Mg–8Gd–3Y–0.5Zr alloy could be explained by higher concentrations of alloying elements, finer grain size and higher percentage of HAGBs in the FSP GW103 alloy. The fine grains and high percentage of HAGBs could provide abundant nucleation sites for precipitation, and the high concentrations of alloying elements rendered high driving force for precipitation and accelerated the growth of the precipitates [24]. Therefore, accelerated precipitation was observed in the FSP GW103 alloy.

On the other hand, as shown in Fig. 6, the volume fraction of the β particles decreased with increasing the annealing temperature at the small temperature range of 400–425 °C, suggesting that the precipitation of β particles in the FSP GW103 alloy was highly sensitive to the temperature. It is well known that the solubility of Gd and Y elements in Mg increased exponentially with temperature [25]. As a result, the solubility of Gd and Y elements could exhibit an obvious variation even at a small temperature range, and therefore the varied volume fraction of β particles at a small temperature range of 400–425 °C was observed.

The precipitation of β particles could exert an effective pinning effect on the grain boundaries, therefore the grain size of the FSP GW103 alloy was unchanged after annealing at different temperatures (Fig. 6(a)–(c)). After superplastic deformation, the growth of both the grains and the β particles occurred. It can be seen that the grain growth in the samples deformed at 400 and 415 °C was not significant (Fig. 6(d)–(e)), while intense grain growth occurred at 425 °C (Fig. 6(f)). This suggests that although the β particles were coarsened during superplastic deformation, the pinning effect of the β particles was still effective at 400 and 415 °C, but

decreased remarkably at 425 °C due to significantly reduced particle number.

4.2. Superplasticity

As shown in Fig. 4(a), the FSP GW103 alloy exhibited a high elongation of 1110% at a strain rate of 1×10^{-3} s^{-1}. This elongation was much higher than those of the Mg–Gd based alloys prepared by hot extrusion [13] and hot rolling [11] with similar high alloy contents.

It is also evident from Fig. 4(a) that the superplasticity of the FSP GW103 alloy varied remarkably at a small temperature range of 400–425 °C. This indicates that the superplasticity of the FSP GW103 alloy was very sensitive to the testing temperature. This could be explained by the marked variation in the volume fraction of the β particles at different temperatures.

In the sample deformed at 400 °C, while a high volume fraction of fine β particles could suppress the grain growth, large local stress concentration could also be generated at the interface between the β particles and the matrix, and therefore the cavities were easy to form. As shown in Fig. 6(d), the large-sized cavities were often associated with the β particles, indicating the large local stress concentration around the particles. In addition, the evident strain softening at the initial stage of deformation at 400 °C as shown in Fig. 3 (a) was also probably suggestive of the early formation and growth of cavities. In this case, the superplasticity was restricted at 400 °C.

In the sample deformed at 425 °C, although the local stress concentration around the β particles decreased due to the significant decrease in the volume fraction of β particles, the grain boundary pinning effect also decreased. In this case, intense grain growth occurred during superplastic deformation. This would result in the strain hardening as shown in Fig. 3(a). Such grain growth could cause stress accumulation at the grain triple junctions, and the cavities were formed, as shown in Fig. 6(f).

In the sample deformed at a medium temperature of 415 °C, the medium volume fraction of β particles could restrict grain growth, but did not produce a large local stress concentration. In this case, the lowest cavity volume fraction and the smallest cavity size were observed. Therefore, the FSP GW103 alloy exhibited the optimum superplasticity at 415 °C. Ma and Mishra [26] observed that the FSP 7075Al deformed at the optimum superplastic temperature exhibited the lowest cavity volume fraction and the smallest cavity size. The present result on the FSP GW103 alloy is consistent with that on the FSP 7075Al.

4.3. Deformation mechanism

Grain boundary sliding (GBS) is considered to be the main superplastic deformation mechanism in fine grained materials and the m value is ~0.5 when GBS is dominant. In the FSP GW103 alloy, the m values of ~0.5 were observed under investigated temperatures and strain rates, indicating that the main superplastic deformation mechanism was GBS. In addition, the uniform and neck-free characteristic of the FSP GW103 alloy was also suggestive of this deformation mechanism as the high m value indicated the high resistance to necking.

It should be noted that, unlike the usually observed deformation surface with clear evidence of GBS [19,27,28], the deformation surface of the FSP GW103 alloy was quite different, as the extensive SBs with a large width were observed. The SBs were also observed in previously studied materials after superplastic deformation [12,29,30]. It is explained that the SBs were the newly exposed grain faces inclined to the specimen surface, and were formed by sliding of grains upward and downward relative to the specimen surface [29]. The deformation surface in the FSP GW103 alloy was similar to that of the Zn–Al two phase alloy after superplastic deformation [31,32], and was formed as a result of diffusion creep, GBS and grain boundary migration (GBM). In the FSP GW103 alloy, during superplastic deformation, besides the deformation of the matrix grains, the mass transfer and phase migration processes could also take place due to the coarsening of β particles. Therefore, the deformation surface of the FSP GW103 alloy might be a complex result of diffusion creep and GBS caused by the motion of both the grains and the β particles.

The constitutive relationship for the superplastic deformation behavior of fine-grained ($d < 10$ μm) magnesium alloys with GBS as the main deformation mechanism can be expressed as [33],

$$\dot{\varepsilon} = 2 \times 10^5 \left(\frac{D_0 Gb}{kT}\right) \exp\left(\frac{-92000}{RT}\right) \left(\frac{b}{d}\right)^3 \left(\frac{\sigma - \sigma_0}{G}\right) \quad (1)$$

where $\dot{\varepsilon}$ is the strain rate, D_o the pre-exponential constant for diffusivity, G the shear modulus, b the Burgers vector, k the Boltzmann's constant, T the absolute temperature, d the grain size, σ the flow stress, and σ_o the threshold stress. Superplastic data of the FSP GW103 alloy were plotted as $\dot{\varepsilon}kTd^3/D_gGb^4$ versus σ/G in Fig. 9. For comparison, a solid straight line predicted by Eq. (1) was also plotted.

It is seen that the normalized superplastic data of the FSP GW103 alloy can fit onto a straight line with a slope of 2, this confirms that GBS controlled by grain boundary self-diffusion is the main superplastic deformation mechanism for the FSP GW103 alloy. On the other hand, the normalized strain rate for the FSP GW103 alloy is about thirty times lower than that for the fine-grained magnesium alloys, indicating that the FSP GW103 alloy has lower deformation kinetics than conventional magnesium alloys.

Previous studies indicated that the presence of high percentage of HAGBs in the FSP alloys could enhance the superplastic deformation kinetics [27,28]. However, enhanced superplastic deformation kinetics was not observed in the present FSP GW103 alloy in spite of the high percentage of HAGBs. This implies that for the FSP GW103 alloy, the main factor that influences superplastic deformation kinetics was not the grain boundary structure. Note that the grain boundary β particles in the FSP GW103 alloy were larger in size and their volume fraction was higher than that in previously studied FSP aluminum and magnesium alloys [16,27]. Such a high volume fraction of large β particles probably resulted in the low superplastic deformation kinetics in the FSP GW103 alloy.

Although the FSP GW103 alloy did not exhibit enhanced deformation kinetics, the maximum superplasticity and the optimum strain rate were higher than those obtained in the Mg–Gd alloys prepared by other processing methods [11,13,14]. This is attrib-

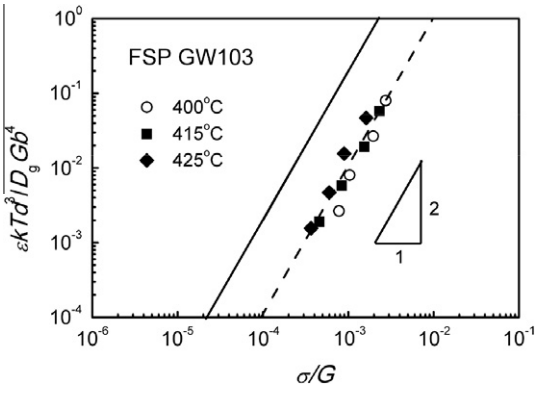

Fig. 9. Variation of $\dot{\varepsilon}kTd^3/D_gGb^4$ with normalized effective stress σ/G for FSP GW 103 alloy.

uted to the following three factors. First, the grain size in the FSP GW103 alloy was finer than that in the previous Mg–Gd alloys [11,13]. It is well documented that fine grain size is beneficial to achieving superplasticity at higher strain rate and lower temperature [34]. Second, it is reported that the HAGB is beneficial to GBS, the predominant HAGBs in the FSP GW103 alloy promoted GBS, increasing the superplastic elongation and the optimum strain rate. Third, as discussed above, a moderate volume fraction of the β particles obtained at an optimum temperature of 415 °C could both restrict grain growth and minimize cavitation, thereby enhancing superplasticity.

5. Conclusions

(1) Fine-grained supersaturated GW103 alloy with a grain size of 6.1 μm and predominant HAGBs was produced by FSP.
(2) Fine β-Mg_5(Gd,Y) particles about ∼1 μm in size precipitated at the grain boundaries in the FSP GW103 alloy during heating before superplastic deformation, and their volume fraction decreased significantly as temperature increased from 400 to 425 °C.
(3) The superplasticity of the FSP GW103 alloy was very sensitive to the deformation temperature, and enhanced superplasticity with a maximum elongation of 1110% was obtained at 415 °C and 1×10^{-3} s^{-1}.
(4) The fine grains, predominant HAGBs, and a moderate volume fraction of the β particles were beneficial to the development of superplasticity in the FSP GW103 alloy.
(5) The FSP GW103 alloy exhibited relatively low superplastic deformation kinetics with GBS as the main deformation mechanism.

Acknowledgements

This work was supported by the National Natural Science Foundation of China under Grant No. 50901075, the National Basic Research Program of China under Grant No. 2011CB606301, and the National Outstanding Young Scientist Foundation of China under Grant No. 50525103.

References

[1] T. Homma, N. Kunito, S. Kamado, Scripta Mater. 61 (2009) 644–647.
[2] R.G. Li, J.F. Nie, G.J. Huang, Y.C. Xin, Q. Liu, Scripta Mater. 64 (2011) 950–953.
[3] A. Singh, Y. Osawa, H. Somekawa, T. Mukai, Scripta Mater. 64 (2011) 661–664.
[4] K. Yamada, Y. Okubo, M. Shiono, H. Watanabe, S. Kamado, Y. Kojima, Mater. Trans. 47 (2006) 1066–1070.
[5] S.M. He, X.Q. Zeng, L.M. Peng, X. Gao, J.F. Nie, W.J. Ding, J. Alloys Comp. 427 (2007) 316–323.
[6] Q.M. Peng, Y.M. Wu, D.Q. Fang, J. Meng, L.M. Wang, J. Alloys Comp. 430 (2007) 252–256.
[7] J. Wang, J. Meng, D.P. Zhang, D.X. Tang, Mater. Sci. Eng. A 456 (2007) 78–84.
[8] Z. Yang, J.P. Li, Y.C. Guo, T. Liu, F. Xia, Z.W. Zeng, M.X. Liang, Mater. Sci. Eng. A 454 (2007) 274–280.
[9] K. Liu, J. Zhang, G. Su, J. Alloys Comp. 481 (2009) 811–818.
[10] R. Kaibyshev, T. Sakai, F. Musin, I. Nikulin, H. Miura, Scripta Mater. 45 (2001) 1373–1380.
[11] L. Li, X.M. Zhang, Y.L. Deng, C.P. Tang, J. Alloys Comp. 485 (2009) 295–299.
[12] Y.J. Wu, L.M. Peng, X.Q. Zeng, J. Mater. Res. 24 (2009) 3596–3602.
[13] X.M. Zhang, L. Li, Y.L. Deng, N. Zhou, J. Alloys Comp. 481 (2009) 296–300.
[14] O.B. Kulyasova, R.K. Islamgaliev, A.R. Kil'mametov, Phys. Met. Metall. 101 (2006) 585–590.
[15] W.J. Kim, B.H. Lee, J.B. Lee, M.J. Lee, Y.B. Park, Scripta Mater. 63 (2010) 772–775.
[16] Q. Yang, B.L. Xiao, Z.Y. Ma, R.S. Chen, Scripta Mater. 65 (2011) 335–338.
[17] Y. Miyahara, Z. Horita, T.G. Langdon, Mater. Sci. Eng. A 420 (2006) 240–244.
[18] J.W. Edington, K.N. Melton, C.P. Cutler, Prog. Mater. Sci. 21 (1976) 61–158.
[19] F.C. Liu, Z.Y. Ma, Scripta Mater. 59 (2008) 882–885.
[20] D.J. Li, Q.D. Wang, Mater. Sci. Eng. A 526 (2009) 150–155.
[21] B.L. Xiao, Q. Yang, J. Yang, W.G. Wang, G.M. Xie, Z.Y. Ma, J. Alloys Comp. 509 (2011) 2879–2884.
[22] Q. Yang, B.L. Xiao, Z.Y. Ma, Metal. Mater. Trans. A (2012) 2094–2109.
[23] A.H. Feng, Z.Y. Ma, Acta Mater. 57 (2009) 4248–4260.
[24] D.A. Porter, K.E. Easterling, Phase Transformations in Metals and Alloys, 2nd ed., Chapman & Hall, London, 1992.
[25] L.L. Rokhlin, Magnesium Alloys Containing Rare Earth Metals, Taylor and Francis, London, 2003.
[26] Z.Y. Ma, R.S. Mishra, Acta Mater. 51 (2003) 3551–3569.
[27] Z.Y. Ma, R.S. Mishra, M.W. Mahoney, R. Grimes, Metal. Mater. Trans. A 36A (2005) 1447–1457.
[28] G.M. Xie, Z.Y. Ma, L. Geng, R.S. Chen, J. Mater. Res. 23 (2008) 1207–1213.
[29] T.R. Chen, J.C. Huang, Metal. Mater. Trans. A 30A (1999) 53–64.
[30] Y.N. Wang, J.C. Huang, Scripta Mater. 48 (2003) 1117–1122.
[31] I.I. Novikov, V.K. Portnoy, T.E. Terentieva, Acta Metall. 25 (1977) 1139–1149.
[32] I.I. Novikov, V.K. Portnoy, V.S. Levchenko, Acta Metall. 29 (1981) 1077–1090.
[33] H. Watanabe, T. Mukai, M. Kohzu, S. Tanabe, K. Higashi, Acta Mater. 47 (1999) 3753–3758.
[34] R.B. Figueiredoa, T.G. Langdon, Scripta Mater. 61 (2009) 84–87.